Fabrication and High Electrocatalytic Activity of Three-Dimensional Porous Nanosheet Pt/Boron-Doped Diamond Hybrid Film

6 AUTHORS, INCLUDING:

Xili Tong
Chinese Academy of Sciences
36 PUBLICATIONS **387** CITATIONS

SEE PROFILE

Peiqiang Li
Iowa State University
24 PUBLICATIONS **357** CITATIONS

SEE PROFILE

Fabrication and High Electrocatalytic Activity of Three-Dimensional Porous Nanosheet Pt/Boron-Doped Diamond Hybrid Film

Xili Tong, Guohua Zhao,* Meichuan Liu, Tongcheng Cao, Lei Liu, and Peiqiang Li

Department of Chemistry, Tongji University, Shanghai 200092, China

Received: April 2, 2009; Revised Manuscript Received: May 18, 2009

A three-dimensional (3-D) Pt nanosheet perpendicular to boron-doped diamond (BDD) hybrid film surface was prepared by the double template method, with a hydrogen bubble template and subsequent metallic Zn template to control the morphology of the Pt catalyst on the BDD surface. The porous Zn nanostructured template on oxygen-terminated BDD was first synthesized by electrodeposition with a concomitant hydrogen bubble as a dynamic template. Then a porous Pt nanostructure was obtained by immersing the Zn nanostructure in H_2PtCl_6 aqueous solution for a typical displacement reaction. Field emission scanning electron microscopy (FESEM) revealed that the morphology of the Zn template obtained was a 3-D porous nanosheet structure perpendicular to the BDD thin film surface, and Pt kept the morphology of the Zn template after the displacement reaction. Energy dispersive spectrometry (EDS) and X-ray diffraction (XRD) revealed that the Pt nanosheet obtained was the classical face-centered cubic (fcc) pattern. Cyclic voltammetry (CV) and electrochemical impedance spectroscopy (EIS) were performed to evaluate methanol electro-oxidation performance of the 3-D Pt nanosheet/BDD electrode. The results indicated that the electrode had a high electrocatalytic ability resulting from the large surface area and porous structure, which efficiently facilitates the transportation of reactants and products, and an antipoisoning ability due to the support activity of BDD.

1. Introduction

Nanoplatinum (Pt) attracts considerable scientific attention as well as industrial attention, because it has widely potential applications in fine chemical synthesis,[1] gas sensing,[2] reduction of pollutant gases emitted from automobiles,[3] and especially methanol oxidation in direct methanol fuel cells (DMFCs).[4,5] One of the most important goals in the synthesis of nanostructure Pt is to develop highly active Pt catalysts. It is well-known that the performance of Pt nanoparticles as the catalyst is influenced not only by the size of nanoparticles but also by their morphology. Furthermore, the morphology, including dimension and shape, of Pt nanoparticles also influences their electronic and magnetic properties.[6] Therefore, the synthesis of platinum with a specific nanostructure has become an area of considerable interest.[7,8] Numerous attempts have been made to obtain different Pt nanostructures, such as multihedral nanoparticles,[9] multipods,[10] nanowires,[11] nanoflowers,[12] and nanocubes.[13] These studies are interesting and provide creative strategies to control the morphology of Pt nanoparticles. Compared to various structures of Pt nanoparticles, the three-dimensional (3-D) porous Pt nanosheet holds a unique structure, which is expected to provide a larger surface area and to facilitate the transport of reactants and products effectively, so that the electrochemical performance of Pt can be greatly improved.[14] However, a 3-D porous Pt nanosheet is seldom reported, so it is significant to prepare and investigate the nanosheet Pt with a 3-D porous structure in detail.

To obtain high activity and stability of the Pt catalyst with nanostructure, the choice of catalyst–support material is an important issue, because the properties of supports are crucial to catalysts.[15] Lots of catalyst–support materials with good corrosion resistance were reported.[16–18] Among these materials,

carbonaceous materials[19–22] have attracted tremendous attention because of the combination of electronic conductivity and surface properties. However, common carbonaceous materials, such as carbon black and carbon nanotube, will undergo irreversible oxidation at non-negligible rates, especially in a harsh working environment, which would deteriorate their performance. Recently, synthetic conductive boron-doped diamond (BDD) thin film fabricated by chemical vapor deposition (CVD) method provides a new type of carbon electrode material, which may overcome this drawback because of its greater chemical stability resulting from its stable tetrahedron structure. Moreover, BDD possesses wide potential window and low and stable background current.[23,24] The unique nature of BDD suggests promising applications in various electrochemical processes, such as electroanalysis,[25] biosensors,[26] and electrochemical degradation for organic pollutants.[27,28] Therefore, it is important to prepare the Pt catalyst loaded on the BDD surface with nanostructure by appropriate methods. Some good methods have been explored, such as emulsion,[29] immerse-reduction,[30] electrodeposition,[31,32] and sol–gel.[33] However, it is difficult to control the morphology of Pt loaded on the BDD surface, and the import of impurity cannot be avoided in previous reports. The reason is mainly due to the inert nature of BDD.

In this study, it is desired to obtain a 3-D Pt nanosheet perpendicular to the BDD thin film surface. To overcome the obstacle resulting from the inert nature of BDD, we will use the hydrogen bubble template and subsequent metallic Zn template to control the morphology of the Pt catalyst loaded on the BDD surface. The proposed double template method is evaluated with electrochemical techniques, FESEM, EDS, and XRD. The performance of the novel 3-D nanosheet perpendicular to the BDD surface electrode for methanol electro-oxidation is also investigated.

* To whom correspondence should be addressed. E-mail: g.zhao@tongji.edu.cn. Tel.: +86-21-65988570-8244. Fax: +86-21-65982287.

SCHEME 1: Schematic Illustration for Making the 3-D Pt Nanosheet Perpendicular to the BDD Thin Film Surface by Using the Double Template Method
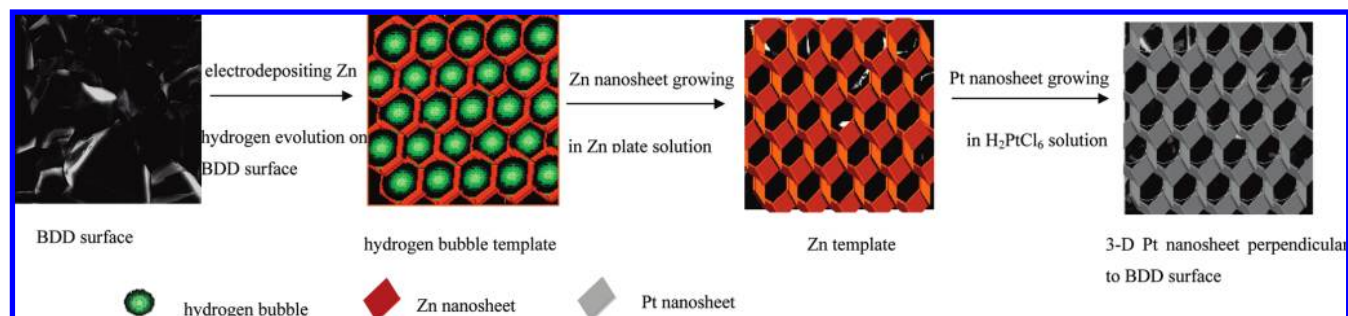
2. Experimental Section

2.1. Materials. ZnCl$_2$, KCl, H$_2$PtCl$_6$, concentrated HNO$_3$ (68%), concentrated H$_2$SO$_4$ (98%), and H$_3$BO$_3$ were obtained commercially of pure analytical grade. All reagents were used as received without further treatment. Electroplate stock solution of zinc salt solution was prepared with double-distilled water, ZnCl$_2$, KCl, and H$_3$BO$_3$.

BDD thin films were deposited on a p-Si(100) surface (area 15 mm × 15 mm) which had been pretreated by polishing with hydrogen for 20 min at low pressure by a wave assisted chemical vapor deposition (MP-CVD) system.[25] The crystallites in these polycrystalline films were of high structural quality, and the sizes ranged from 5 to 10 μm.

2.2. Preparation of a 3-D Porous Nanosheet Pt/BDD Hybrid Film by the Double Template Method. The electrochemical experiments were carried out on a CHI 660C electrochemical workstation (CH Instrument, U.S.) at room temperature (20 ± 1 °C). A traditional three-electrode system with a platinum plane with a surface area of 2 cm^2 was used as the auxiliary electrode, a saturated calomel electrode (SCE) as the reference, and a BDD electrode (with the apparent BDD surface area limited to 0.09 cm^2 by the O-ring) as the working electrode.

The electrodeposition on the oxygen-terminated BDD electrode was carried out in a 0.5 M ZnCl$_2$/6 M KCl/0.5 M H$_3$BO$_3$ solution without agitation. A constant current, 0.15 A cm^{-2}, was applied at room temperature for 30 s. The modified BDD electrode was rinsed with deionized water and then subjected to 5 mM H$_2$PtCl$_6$ aqueous solution for a typical displacement reaction for 6 h. The treated modified BDD electrode was kept in 0.1 M H$_2$SO$_4$ before the electrochemical experiments.

2.3. Characterization. Field emission scanning electron microscopy (FESEM) was conducted with a Hitachi S-4700 instrument equipped with energy dispersive spectrometry (EDS). X-ray diffraction (XRD) patterns were obtained on a D/max 2550 VB+/PC (Rigaku) with Cu Kα radiation.

2.4. Test for Electrochemical Property. Electrochemical measurements for methanol electro-oxidation included cyclic voltammetry (CV) and electrochemical impedance spectroscopy (EIS) and were examined in a 0.1 M H$_2$SO$_4$/1.5 M CH$_3$OH solution without agitation at room temperature. The amplitude of modulation potential for the EIS measurements was 5 mV, and the frequency varied from 100 kHz to 10 mHz.

3. Results and Discussion

3.1. Construction of a 3-D Pt Nanosheet Structure on the BDD Surface. The construction flowsheet of a 3-D porous Pt nanosheet perpendicular to the BDD surface is shown in Scheme 1. Polycrystalline diamond layers were synthesized on a silicon

high purity p-type wafer with low cost in a conventional reactor. The surface termination may be one of the most important issues for controlling the electrochemical behavior of BDD.[34] The deposited BDD surface obtained is hydrogen-terminated with a hydrophobic character, and it is stable in the air without any apparent degradation for several months. However, this hydrophobic surface is not suitable for metal nucleation growth. To obtain oxygen-terminated BDD, the deposited BDD electrode after ultrasonic cleaning was first immersed in aqua regia at 90 °C for 10 min and then anodic oxidized in 1 M H$_2$SO$_4$ at 3.2 V (vs SCE) for 45 min. Oxidation of hydrogen-terminated diamond leads to the BDD electrode with a final surface composition composed of ether (C−O−C), carbonyl (C=O), and surface hydroxyl (C−OH) groups.[35] This new surface is hydrophilic, which is beneficial to metal nucleation growth.[36] The change of contact angle for BDD before and after oxidation is presented in S1 of the Supporting Information.

A 3-D foam structure of copper and tin with nanodendritic walls has been fabricated using the concurrence generation of hydrogen bubble as a dynamic template in the electrodeposition process at high cathodic current densities.[37,38] In general, to obtain a stable 3-D porous morphology of metal species loaded on the surface when using hydrogen bubble as a template, it is necessary to ensure that most hydrogen bubbles come from the surface. It is well-known that the BDD electrode has a high overpotential for hydrogen evolution in aqueous solution, while Pt has a low overpotential for hydrogen evolution, so it is not feasible to construct 3-D porous Pt on the BDD surface by direct electrodeposition of Pt with a hydrogen template. To overcome this obstacle, Zn was chosen as a bridge to construct stable and regular 3-D porous morphology of Pt on the BDD surface since Zn was one of the active metals with higher hydrogen overpotential compared with BDD (Figure S2 in Supporting Information). A 3-D porous Zn nanosheet perpendicular to BDD surface was first obtained by hydrogen bubble template because of the growth preference of zinc crystal.[39] Then, a 3-D porous Pt nanosheet perpendicular to BDD surface was achieved by a galvanic displacement reaction, eq 1, with metallic Zn as a template. More information is available in Figure S3 in the Supporting Information.

$$H_2PtCl_6 + 3Zn \rightarrow 3ZnCl_2 + Pt + H_2\uparrow \qquad (1)$$

3.2. Physical and Chemical Characteristics. Figure 1 shows FESEM and EDS images of the extracted samples. The crystallites in polycrystalline BDD films were of high structural quality, and the sizes were in the range of 5−10 μm in Figure 1a. Figure 1b,c shows the images of 3-D porous Zn nanosheet perpendicular to BDD surface. The length and thickness of Zn

A 3-D Porous Nanosheet Pt/BDD Hybrid Film

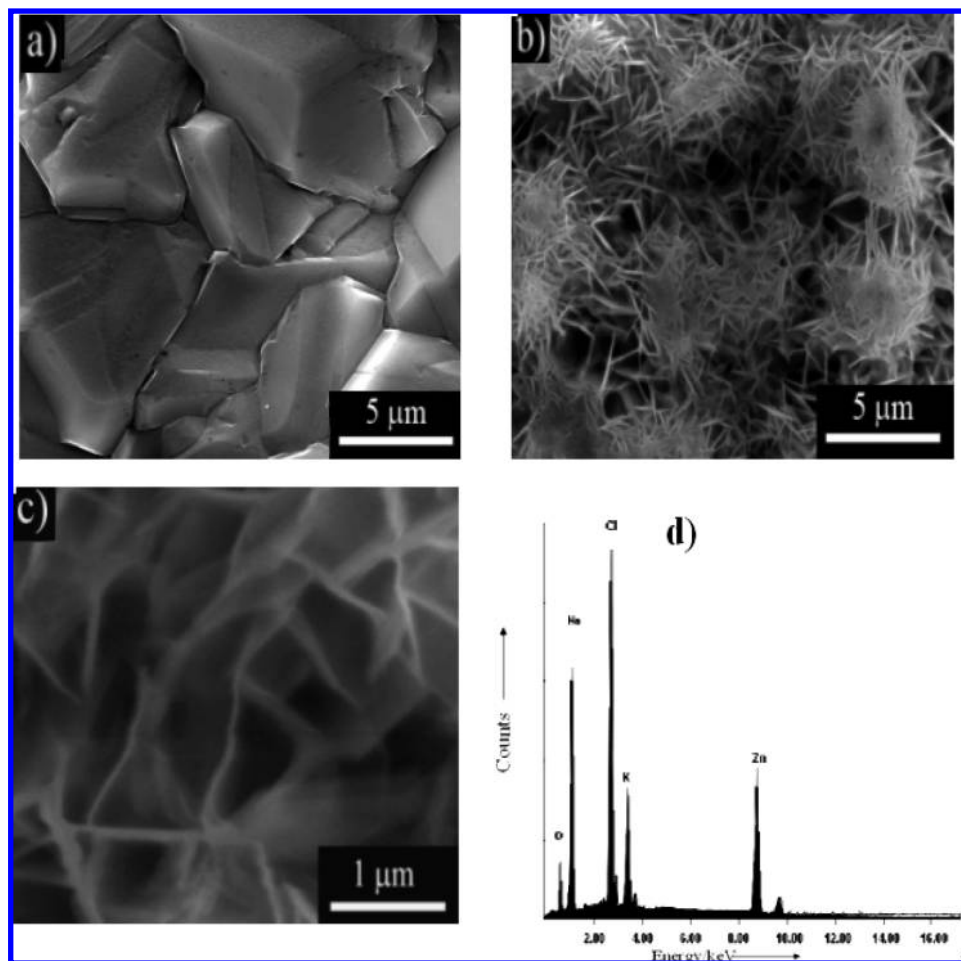*J. Phys. Chem. C, Vol. 113, No. 31, 2009* **13789**

Figure 1. FESEM (a) image of BDD and FESEM (b) and EDX (c) images of the Zn nanosheet on the BDD thin film surface.

nanosheet were about 1 μm and 10 nm, respectively. In the experiment, the nucleation and growth of Zn nanosheet uniformly went along the direction perpendicular to the surface. This interesting result may come from the reason that the Zn nanosheet would maintain the most stable crystal structure, subjected to the lowest hydrogen bubble attack in the electrodeposition process. From the EDS image, the peaks correspond to Zn, Cl, and other elements. Shin and Liu reported[37] that the electrodeposition process always created a 3-D dendritic structure with the ramification of metal, which is easily collapsed under harsh conditions. However, in the present nanosheet, Zn nanosheet walls do not exhibit visible pores or seams caused by high concentration of Zn^{2+} and Cl^-, so that the drawback of the porous dendritic structure[40,41] is avoided.

Figure 2 shows FESEM and EDS images of the extracted samples after a galvanic displacement. SEM shows that Pt keeps the 3-D porous naonosheet morphology of Zn because Zn acts as a template. This novel morphology is quite different from that of the Pt particle of direct electrodeposition on the BDD electrode.[31,32] The length and thickness of the Pt nanosheet are about 1 μm and 10 nm, respectively. The pores may behave as individual nanoscale reactors, and the sizes of pores are large enough for the penetration of reactants and products. According to EDS image in Figure 2, all of the peaks correspond to Pt on the BDD surface, indicating that metal Zn is completely displaced.

The extracted samples are further characterized by XRD, and their XRD patterns are shown in Figure 3. In the case of BDD, the diffraction peaks at 29.20 and 44.60 in the XRD plot

correspond to the Si surface and diamond film, respectively (Figure 3a). As the electrodeposition continues, the surface of BDD is covered with 3-D porous metallic Zn networks, which results in a dramatic decrease in the characteristic diffraction peaks of Si and diamond. Metallic Zn with a hexagonal close-packed (HCP) pattern is demonstrated by the characteristic Zn diffraction peaks (002), (100), (101), and (102). Among these diffraction peaks, the intensity of diffraction peak (101) is much larger than that of other perks, indicating that metallic Zn goes along the [101] direction on the BDD surface. As a result, metallic Zn prefers to form the morphology of the nanosheet, rather than the morphology of highly porous ramified wall,[37] which is confirmed by SEM characterization in Figure 1b,c. Pt nanosheets are obtained through displacement reaction, eq 1, in which Zn nanosheet acts as the template. The Pt nanosheet obtained is the face-centered cubic (fcc) pattern (space group: Fm3m) demonstrated by the remaining diffraction peaks (111), (200), and (220), and no other unknown diffraction peak appears in Figure 3c. This confirms that the Pt nanosheet synthesized by the double template method is crystallized in a phase similar to bulk Pt.

Figure 4 presents the cyclic voltammograms (CVs) of Pt wire and the Pt nanosheet/BDD sample in a 0.1 M H_2SO_4 solution at a potential scan rate of 50 mV s^{-1}. Three pairs of reversible peaks corresponding to the hydrogen adsorption and desorption are observed in the potential range between -0.4 and 0 V (vs SCE), rather than a single broad peak, which is indicative of multiple exposed crystallographic planes. In Figure 4a, the oxidation and reduction potential of the Pt nanosheet shifts
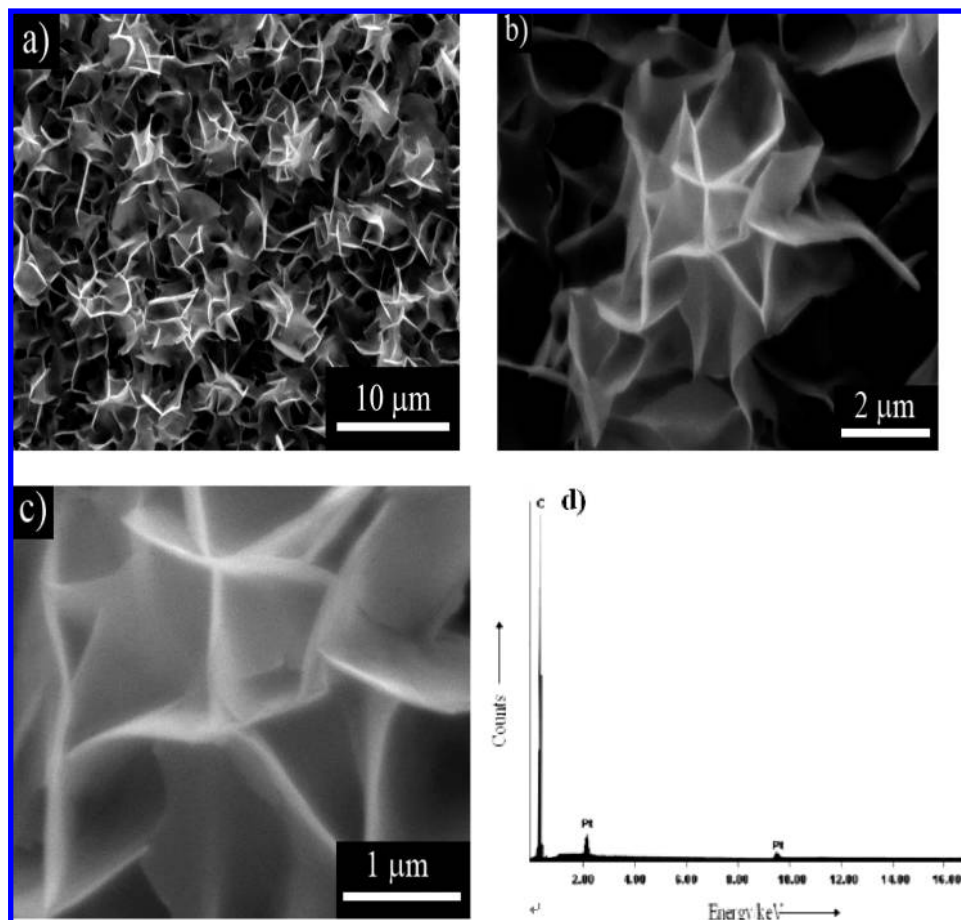
Figure 2. FESEM (a, b, c) and EDX (d) images of the Pt nanosheet on the BDD thin film surface.
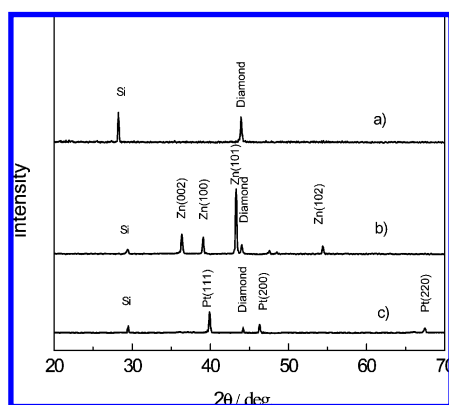

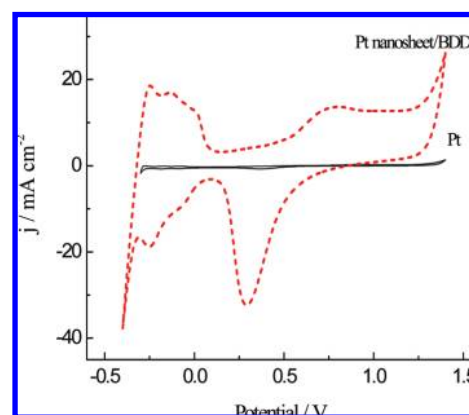**Figure 3.** XRD patterns of BDD (a), Zn/BDD (b), and the Pt nanosheet/BDD (c).

Figure 4. Cyclic voltammogram of pristine Pt and the Pt nanosheet/BDD in a 0.1 M H_2SO_4 solution at a scan rate of 50 mV s^{-1}.

negatively in comparison with those of polycrystalline Pt, which illustrates that the Pt nanosheet has more active electrocatalytic capability. Hydrogen adsorption and desorption is a powerful technique to determine the active surface area of a Pt electrode.[42] The integrated intensity of the peaks represents the number of Pt sites available for hydrogen adsorption/desorption, that is, the actual surface area. By means of hydrogen adsorption—desorption methods and with CV,[43] the electrochemical surface area (S_{EL}) of platinum can be measured. Q_H represents the number of Pt sites available for hydrogen adsorption/desorption (mC cm^{-2}). Q_H of the Pt nanosheet on BDD measured under the electro-adsorption curve for hydrogen is 52.4 mC cm^{-2}, and atomic absorption spectrometry approach analysis[32] gives Pt nanosheet loading of 0.238 mg

cm^{-2}. On the basis of the Q_H value and Pt loading, S_{EL} of Pt on BDD film is calculated as follows:

$$S_{EL} = Q_H/(Q_{ref} \times \text{Pt loading})$$

S_{EL} is in cm^2 mg^{-1} when the Pt loading is in mg cm^{-2}. That $Q_{ref} = 0.21$ mC cm^{-2} is generally accepted for polycrystalline Pt electrodes.[44] The value of S_{EL} is obtained as 104.8 m^2 g^{-1} for the Pt nanosheet on BDD film, while $S_{EL} = 97.6$ m^2 g^{-1} for commercial products and $S_{EL} = 99$ m^2 g^{-1} for Pt nanoflowers on carbon paper.[43] This result indicates that more Pt is available electrochemically at the Pt nanosheet on BDD

A 3-D Porous Nanosheet Pt/BDD Hybrid Film
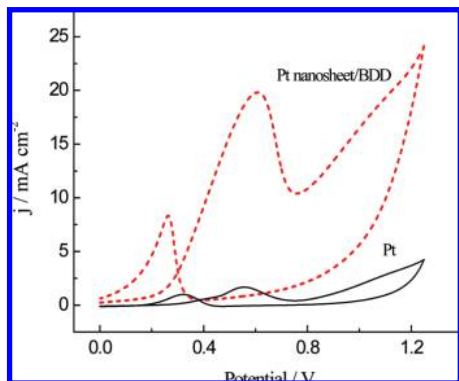
J. Phys. Chem. C, Vol. 113, No. 31, 2009 **13791**

Figure 5. Cyclic voltammogram of pristine Pt and the Pt nanosheet/BDD in a 0.1 M H_2SO_4/1.5 M CH_3OH solution at a scan rate of 50 mV s^{-1}.

film surface than at the surface of the commercial carbonaceous materials.

3.3. Methanol Electro-oxidation. Figure 5 presents the CVs of polycrystalline Pt and Pt nanosheet/BDD samples at a potential scan rate of 50 mV s^{-1}. The current density is calculated from the electrochemical active surface area. The onset potential of methanol oxidation at the Pt nanosheet (about 0.2 V) (vs SCE) is lower than that at polycrystalline Pt (about 0.32 V) (vs SCE). This result indicates that the Pt nanosheet/BDD has higher electrocatalytic activity because of the size effect of the Pt nanosheet and the effect of excellent support activity of BDD. The peak current density of methanol electro-oxidation in a forward scan of nanosheet Pt is 13 times that of polycrystalline Pt. With a porous nanostructure, the Pt nanosheet has more reactive active sites, and more reactants participate in the reaction because of free diffusion, which results in a higher current density. In methanol electro-oxidation, the anodic peak in the reverse scan is usually attributed to the removal of intermediate carbonaceous residues formed on the catalyst during the forward scan. Therefore, the ratio of two anodic current densities, If/Ib, is commonly used to describe the catalyst susceptibility to poisoning.[45,46] In the case of polycrystalline Pt, this value is 1.5, which indicates that a significant number of methanol molecules are only partially oxidized in the forward scan. However, the Pt nanosheet/BDD exhibits a larger If/Ib ratio, 2.8. This higher poison-resistant ability of the Pt nanosheet/BDD hybrid electrode is related not only to the unique structure of the Pt nanosheet but also to plenty of —OH on the surface of BDD.[47] Besides, the electrocatalytic ability decreases less than 10% after this electrode is kept in the air for two months.

Figure 6 illustrates two Nyquist plots of the pristine Pt and Pt nanosheet/BDD at the potential of 0.375 V. From Figure 6a, electrochemical control of methanol electro-oxidation on the pristine Pt electrode is found, but in the case of the Pt nanosheet/BDD electrode, the reaction process of methanol electro-oxidation is more complicated.[48] On the other hand, the diameter of a semicircle of the Pt nanosheet sample is only 5% of that of the pristine Pt sample. In Figure 6b, the inset plot is the magnified section of the high-frequency zone of the Nyquist plot of the Pt nanosheet/BDD. A typical pseudoinductive behavior[49,50] was observed in the impedance plot, where a large arc at high frequency is accompanied by a small arc in the fourth quadrant at low frequency. A feasible explanation for the occurrence of inductive behavior during methanol oxidation can be extracted by comparing these two processes: initially, the reaction sites are covered with an adsorbed CO layer generated from methanol dehydrogenation. As potential increases, some of the weakly adsorbed CO begins to be oxidized, producing
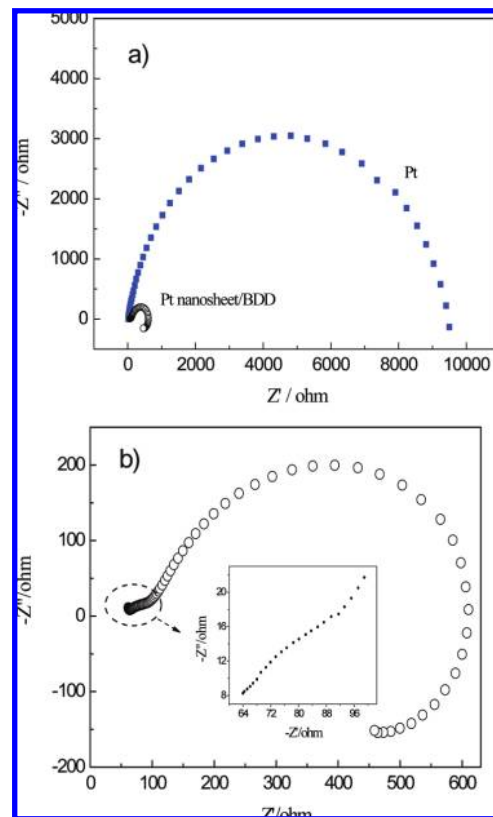

Figure 6. EIS of Pt and the Pt nanosheet/BDD in a 0.1 M H_2SO_4/1.5 M CH_3OH solution (a) and the magnified EIS plot of the Pt nanosheet/BDD in (a).

pores in the adsorbed CO layer. Subsequent methanol oxidation then can take place within these pores. This electrochemical behavior is similar to pseudoinductive behavior during the corrosion test, which was caused by pitting in the protection layer and subsequent corrosion of metal within the pores of the protection layer. This interesting result shows that this novel Pt nanosheet/BDD hybrid electrode has high activity for methanol electro-oxidation, which resulted from the unique construction of an open 3-D porous Pt nanosheet/BDD electrode. In addition, the resistance in the high-frequency zone presented the relaxation of Pt nanosheet surface, which is typical of EIS character of the embedded electrode.

4. Conclusion

Construction of a 3-D porous Pt nanosheet perpendicular to the BDD hybrid film surface was achieved through a simple and facile double template method, which may be extended to other noble metals with a porous nanostructure on the BDD surface. The physical and electrochemical results indicated that the 3-D porous Pt nanosheet perpendicular to the BDD surface electrode had a high catalytic ability and antipoisoning ability for methanol electro-oxidation, because of the larger electrochemical active area and porous structure and the activity of BDD substrate. Since the 3-D porous nanosheet structure provides a large surface area and effectively facilitates the transportation of reactants and products in reaction channels, which is especially desirable for a catalyst in various electrochemical processes, this novel electrode with a unique surface structure will be very attractive in fuel cells, sensors, and nanoelectronics.

Tong et al.

Supporting Information Available: A study of the contact angle BDD surface before and after oxidation treatment, hydrogen evolution reaction at the Zn electrode and BDD electrode, and a chronopotentiometry image of the BDD electrode in the constant current electrodeposition Zn process. This material is available free of charge via the Internet at http://pubs.acs.org.

References and Notes

(1) Diezi, S.; Ferri, D.; Vargas, A.; Mallat, T.; Baiker, A. *J. Am. Chem. Soc.* **2006**, *128*, 4048.

(2) Kolmakov, A.; Klenov, D. O.; Lilach, Y.; Stemmer, S.; Moskovits, M. *Nano Lett.* **2005**, *5*, 667.

(3) Roucoux, A.; Schulz, J.; Patin, H. *Chem. Rev.* **2002**, *102*, 3757.

(4) Winter, M.; Brodd, R. J. *Chem. Rev.* **2004**, *104*, 4245.

(5) Zhao, Y.; Fan, L.; Zhong, H.; Li, Y.; Yang, S. *Adv. Funct. Mater.* **2007**, *17*, 1537.

(6) Chen, J. Y.; Herricks, T.; Xia, Y. N. *Angew. Chem., Int. Ed.* **2005**, *44*, 2589.

(7) Song, Y. J.; Steen, W. A.; Pena, D.; Jiang, Y. B.; Medforth, C. J.; Huo, Q. S.; Pincus, J. L.; Qiu, Y.; Sasaki, D. Y.; Miller, J. E.; Shelnutt, J. A. *J. Am. Chem. Soc.* **2004**, *126*, 635.

(8) Narayanan, R.; El-Sayed, M. A. *J. Am. Chem. Soc.* **2004**, *126*, 7194.

(9) Ahmadi, T. S.; Wang, Z. L.; Green, T. C.; Henglein, A.; El-Sayed, M. A. *Science* **1996**, *272*, 1924.

(10) Teng, X.; Yang, H. *Nano Lett.* **2005**, *5*, 885.

(11) Lee, E. P.; Peng, Z.; Cate, D. M.; Yang, H.; Campbell, C. T.; Xia, Y. *J. Am. Chem. Soc.* **2007**, *129*, 10634.

(12) Sun, S.; Yang, D.; Villers, D.; Zhang, G.; Sacher, E.; Dodelet, J. *Adv. Mater.* **2008**, *20*, 571.

(13) Yang, W.; Wang, X.; Yang, F.; Yang, C.; Yang, X. *Adv. Mater.* **2008**, *20*, 2579.

(14) Xie, F.; Meng, H.; Shen, P. *Electrochim. Acta* **2008**, *53*, 5039.

(15) Ganesan, R.; Lee, J. S. *Angew. Chem., Int. Ed.* **2005**, *4*, 6557.

(16) Vinodgopal, K.; Haria, M.; Meisel, D.; Kamat, P. *Nano Lett.* **2004**, *4*, 415.

(17) Su, F.; Zeng, J.; Bao, X.; Yu, Y.; Lee, J. Y.; Zhao, X. S. *Chem. Mater.* **2005**, *17*, 3960.

(18) Wen, Z.; Wang, Q.; Li, J. *Adv. Funct. Mater.* **2008**, *18*, 959.

(19) Vinodgopal, K.; Haria, M.; Meisel, D.; Kamat, P. *Nano Lett.* **2004**, *4*, 415.

(20) Su, F.; Zeng, J.; Bao, X.; Yu, Y.; Lee, J. Y.; Zhao, X. S. *Chem. Mater.* **2005**, *17*, 3960.

(21) Wen, Z.; Wang, Q.; Li, J. *Adv. Funct. Mater.* **2008**, *18*, 959.

(22) Cui, G.; Zhi, L.; Thomas, A.; Kolb, U.; Lieberwirth, I.; Müllen, K. *Angew. Chem., Int. Ed.* **2007**, *46*, 3464.

(23) Preechaworapun, A.; Ivandini, T. A.; Suzuki, A.; Fujishima, A.; Chailapakul, O.; Einaga, Y. *Anal. Chem.* **2008**, *80*, 2077.

(24) Song, Y.; Swain, G. M. *Anal. Chem.* **2007**, *79*, 2412.

(25) Zhao, G.; Tong, X.; Hu, Z.; Xiao, X.; Li, D. *Electrochim. Acta* **2008**, *53*, 4283.

(26) Geng, R.; Zhao, G.; Liu, M.; Li, M. *Biomaterials* **2008**, *29*, 2794.

(27) Louhichi, B.; Ahmadia, M. F.; Bensalah, N.; Gadri, A.; Rodrigo, M. A. *J. Hazard. Mater.* **2008**, *158*, 430.

(28) Deligiorgis, A.; Xekoukoulotakis, N. P.; Diamadopoulos, E.; Mantzavinos, D. *Water Res.* **2008**, *42*, 1229.

(29) Siné, G.; Fóti, G.; Comninellis, C. *J. Electroanal. Chem.* **2006**, *595*, 115.

(30) Nishio, K.; Masuda, H. *J. Electroanal. Chem.* **2001**, *514*, 35.

(31) Honda, K.; Yoshimura, M.; Rao, T. N.; Tryk, D. A.; Fujishima, A.; Yasui, K.; Sakamoto, Y.; Riedo, B.; Dietler, G.; Enea, O. *Thin Solid Films* **2005**, *488*, 82.

(32) Bennett, J. A.; Show, Y.; Wang, S.; Swain, G. M. *J. Electrochem. Soc.* **2005**, *152* (2), E184.

(33) Salazar-Banda, G. R.; Suffredini, H. B.; Calegaro, M. L.; Tanimoto, S. T.; Avaca, L. A. *J. Power Sources* **2006**, *162*, 9.

(34) Szunerits, S.; Jama, C.; Coffinier, Y.; Marcus, B.; Delabouglise, D.; Boukherroub, R. *Electrochem. Commun.* **2006**, *8*, 1185.

(35) Ferro, S.; Colle, M. D.; Battisti, A. D. *Carbon* **2005**, *43*, 1191.

(36) Hull, R. V.; Li, L.; Xing, Y.; Chusuei, C. C. *Chem. Mater.* **2006**, *16*, 1780.

(37) Shin, H. C.; Liu, M. L. *Chem. Mater.* **2004**, *16*, 5461.

(38) Shin, H. C.; Dong, J.; Liu, M. L. *Adv. Mater.* **2003**, *15*, 1610.

(39) Fukami, K.; Nakanishi, S.; Yamasaki, H.; Tada, T.; Sonoda, K.; Kamikawa, N.; Tsuji, N.; Sakaguchi, H.; Nakato, Y. *J. Phys. Chem. C* **2007**, *111*, 1150.

(40) Shin, H. C.; Liu, M. L. *Adv. Funct. Mater.* **2005**, *15*, 582.

(41) Li, Y.; Song, Y.; Yang, C.; Xia, X. *Electrochem. Commun.* **2007**, *9*, 981.

(42) Kardash, D.; Korzeniewski, C. *Langmuir* **2000**, *16*, 8419.

(43) Sun, S.; Yang, D.; Villers, D.; Zhang, G.; Sacher, E.; Dodelet, J. *Adv. Mater.* **2008**, *20*, 571.

(44) Woods, R. *Electroanalytical Chemistry*; Band, A. J., Ed.; CRC Press: New York, 1976.

(45) Liu, Z.; Ling, X. Y.; Su, X.; Lee, J. Y. *J. Phys. Chem. B* **2004**, *108*, 8234.

(46) Ge, X.; Wang, R.; Liu, P.; Ding, Y. *Chem. Mater.* **2007**, *19*, 5827.

(47) Musthafa, O. T. M.; Sampath, S. *Chem. Commun.* **2008**, 67.

(48) Hsing, I.; Wang, X.; Leng, Y. *J. Electrochem. Soc.* **2002**, *149* (5), A615.

(49) Armstrong, R. D.; Henderson, M. *J. Electroanal. Chem.* **1972**, *39*, 81.

(50) Keddam, M.; Mattos, O. R.; Takenouti, H. *J. Electrochem. Soc.* **1981**, *128*, 257.